IV International Conference on Particle-based Methods – Fundamentals and Applications
PARTICLES 2015
E. Oñate, M. Bischoff, D.R.J. Owen, P. Wriggers & T. Zohdi (Eds)

# EFFECT OF BOUNDARY CONDITION APPLYING TYPE ON HEAT TRANSFER MODELING VIA DOUBLE SPECIES LATTICE BOLTZMANN METHOD

**M. MOHAMMADI-AMIN[1]*, M. BUSTANCHY[2]**

[1] Aerospace Research Institute
Tehran 1465774111, Iran
mmohammadi@ari.ac.ir

[2] University of Tehran
Kish International Campus
Kish Island, Iran

**Key words:** Natural Convection, Thermal Lattice Boltzmann, Nusselt Number.

**Abstract.** The principle objective of the present study is to solve the velocity and temperature fields using two different distribution functions double species thermal lattice Boltzmann method (TLBM). The study is carried out for a wide range of Rayleigh numbers, velocity and temperature distributions as well as Nusselt numbers were obtained for the Rayleigh numbers ranging from $10^3$ to $10^6$ with the Prandtl number around 0.718 for air. In this simulation, the Boussinesq approximation applied to the buoyancy force term. Also we evaluate the order of derivatives' effect on the accuracy of macroscopic values. So, we applied this method for all of boundary condition types same as no slip, constant temperature and adiabatic walls in two different TLBM model and macroscopic states. We showed that boundary condition applying type has not any difference and based on computer code, we can use both of them with minimum term of derivatives. Results are presented in form of streamline and isothermal plots as well as the variation of average Nusselt number at the walls and domain and compared with commercial CFD softwares and other established methods referenced through literature. A good agreement is obtained between the current solution and the previous works and it shows that we can use double species TLBM with minimum terms of derivatives on a macroscopic and TLBM parameters in boundary conditions discretization. Results are in a good independency from the grids and size of mesh. Finally it is showed that we can solve the first rows and corners (the nodes on the body) of grid with macroscopic terms then continue for other lattices with TLBM to improve accuracy and save the time.

## 1 INTRODUCTION

For more than a decade, lattice Boltzmann method (LBM) has been demonstrated to be a very effective numerical tool for a broad variety of complex fluid flow phenomena that are problematic for conventional methods [1, 2]. Compared with traditional computational fluid dynamics, LBM algorithms are much easier to be implemented especially in complex geometries and multi component flows [1]. LBM is an ideal mesoscopic approach to solve nonlinear macroscopic conservation equations due to its simplicity and parallelization. For incompressible isothermal flows, the LBM is found to be at least as stable, accurate and computationally efficient, as traditional computational methods and has achieved excellent success in different application areas such as multiphase flow and complex fluid phenomena [3]. Natural convection in a porous enclosure with vertical partitioned walls at different temperatures is frequently encountered in many practical applications, such as insulation for buildings, industrial cold-storage installations, electronic cooling and heat exchangers [4].

Peng (2003), evaluated a 3-D incompressible thermal lattice Boltzmann model (TLBM) and its application to simulate natural convection in a cubic cavity by using two different particle velocity models of D3Q15 and D3Q19 in thermal models and compared results by Navier-Stokes solver [3]. Changqing et.al (2007) simulated a transient natural convection in square cavity with incompressible TLBM. They were shown that as Rayleigh number increase, the flow field gets more intensively [5]. Anilkumar and Jilani (2008) evaluated a natural convection heat transfer enhancement in a closed cavity with partition utilizing Nano-fluids. Their study was carried out numerically for a range of Rayleigh number ($Ra$), partition heights and aspect ratio in two dimensional for flow and temperature distributions [2]. Azwadi and Tanahashi (2008) presented relations for development of 2-D and 3-D double-population TLBM and investigated natural convection flows in a cubic cavity and 2-D porous plate Couette flow. They found a new lattice of four-velocity (2-D) and eight-velocity (3-D) models for internal energy density distribution function and developed this method for analyzing problems where the viscous and compressive heating effects were negligible [6]. The objective of this work is to investigate the effect of boundary condition applying type, macroscopic state and distribution functions, on heat transfer modeling via a lattice model.

## 2 GOVERNING EQUATIONS

In kinetic theory, the evolution of the single-particle density distribution function $[f(t, \vec{x}, \vec{c})]$ which represents the probability density of a particle with unit mass moving with velocity $\vec{c}$ at point $\vec{x}$ at time $t$, is governed by the Boltzmann equation [7]:

$$\frac{\partial f}{\partial t} + \vec{c} \,.\nabla f = \frac{\partial_e f}{\partial t} \tag{1}$$

where the term on the right hand side represents the collision operator. An approximation of this complicated operator is the so-called BGK or the single-relaxation time model [7].

The Boltzmann equation with the Bhatnagar-Gross-Krook (BGK), or single-relaxation-time approximation [6] with external force is given by

$$\frac{\partial f}{\partial t} + \vec{c} \,.\nabla f = -\frac{1}{\tau_f}\,(f - f^{eq}) + F_f \tag{2}$$

where $F_f$ is the external force and $f^{eq}$ is the local Maxwell-Boltzmann equilibrium distribution function given by

$$f^{eq} = \rho\left(\frac{1}{2\pi RT}\right)^{\frac{D}{2}} exp\left\{-\frac{(c-u)^2}{2RT}\right\} \tag{3}$$

where $R$ is the ideal gas constant, $D$ is the dimension of the space, and $\rho$ , $\vec{u}$, and $T$ are the macroscopic density, velocity, and temperature respectively. The macroscopic variables $\rho$ , $\vec{u}$, and $T$ can be evaluated as the moment to the distribution function as follow

$$\rho = \int f d\vec{c} \tag{4}$$

$$\rho\vec{u} = \int \vec{c} f d\vec{c} \tag{5}$$

$$\frac{D\rho RT}{2} = \int \frac{1}{2} f(\vec{c} - \vec{u})^2 d\vec{c} \tag{6}$$

The pressure is determined by equation of state P= ρ/3 and the sound speed is $c_s = \sqrt{1/3}$. By applying Chapmann-Enskog expansion [8], the above equations can lead to macroscopic continuity, momentum and energy equation. However the Prandtl number ($Pr$) obtained is fixed to a constant value [9]. This is caused by the use of single relaxation time in the collision process. The relaxation time of energy carried by the particles to its equilibrium is different to that of momentum. Therefore we need to use a different two relaxation times to characterize the momentum and energy transport. This is equivalent in introducing a new distribution function to define energy. To obtain the new distribution function modeling energy transport, the internal energy density distribution function is introduced as [6]

$$g = \frac{(c-u)^2}{DR} f \tag{7}$$

Substituting Eq. (7) into Eq. (2) results in

$$\frac{\partial g}{\partial t} + \vec{c}\frac{\partial g}{\partial x} = -\frac{1}{\tau_g}(g - g^{eq}) + F_g + f_q \tag{8}$$

where

$$g^{eq} = \frac{(c-u)^2}{DR} f^{eq} \tag{9}$$

$$F_g = \frac{(c-u)^2}{DR} F_f \tag{10}$$

Eq. (7) represents the internal energy carried by the particles and therefore Eq. (8) can be called as the evolution equation of internal energy density distribution function [6]. The macroscopic variables can thus be redefined in term of distribution function $f$ and $g$ as

$$\rho = \int f d\vec{c} \tag{11}$$

$$\rho\vec{u} = \int \vec{c} f d\vec{c} \tag{12}$$

$$\rho T = \int g d\vec{c} \tag{13}$$

where a new relaxation time $\tau_c$ is introduced for simplifying the collision term, and the local equilibrium distribution function is defined by Eq. (8). We have recently shown that in the limit of incompressibility ($Ma \ll 1.0$) and for the cases when the compression work and viscous heat dissipation are negligibly small, Eq. (8) can be simplified to [7]

$$\frac{\partial g}{\partial t} + \vec{c}.\nabla g = -\frac{1}{\tau_g}(g - g^{eq}) \tag{14}$$

The kinetic viscosity ($\vartheta$) is related to related to the relaxation time through the same equation of

$$\vartheta = \frac{2\tau_f - 1}{6} \tag{15}$$

and the thermal diffusivity ($\alpha$) is given by [7]

$$\alpha = \tau_g RT \tag{16}$$

The macroscopic quantities such as density, velocity and temperature are then obtained through moment integrations of distribution function. We have also shown that the macroscopic conservation equations of mass, momentum, and energy can be recovered from the Boltzmann BGK equations (2) and (14) through the Chapman-Enskog expansion [7].

## 3 DISCRETIZATION METHOD

In order to apply the lattice Boltzmann scheme into the digital computer, we need to discretize the evolution equation of the continuous lattice Boltzmann BGK equation for the momentum and energy. Expanding both of the equilibrium distribution function up to $u^2$ results in

$$f^{eq} = \rho\left(\frac{1}{2\pi RT}\right)^{\frac{1}{2}} exp\left\{-\frac{c^2}{2RT}\right\}\left[1 + \frac{\vec{c}.\vec{u}}{RT} + \frac{(\vec{c}.\vec{u})^2}{2(RT)^2} - \frac{u^2}{2RT}\right] \tag{17}$$

$$g^{eq} = \rho T\left(\frac{1}{2\pi RT}\right)^{\frac{1}{2}} exp\left\{-\frac{c^2}{2RT}\right\}\left[1 + \frac{\vec{c}.\vec{u}}{RT}\right] \tag{18}$$

The equations are discretized by energy method, reported in literature. The D2Q9 lattice for 2-D density and internal energy distribution function is shown in Fig.1 [6].

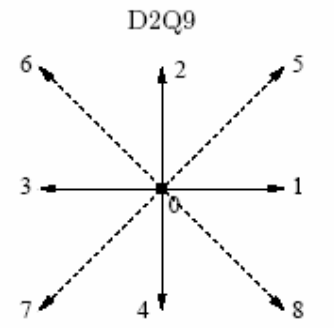


Figure 1: D2Q9 Lattice structure with nine velocities for 2-D distribution function

Eq. (18) is obtained by assuming that at low Mach number flow (incompressible flow), the higher order of $O(u^2)$ and viscous heat dissipation can be neglected [6]. For the two dimensional case, the resultant discrete velocity and thermal equations are given by [7]

$$\frac{\partial f_i}{\partial t} + \vec{c_i} \,.\nabla f_i = -\frac{1}{\tau_f}\left(f_i - f_i^{eq}\right) \tag{19}$$

$$\frac{\partial g_i}{\partial t} + \vec{c_i} \,.\nabla g_i = -\frac{1}{\tau_g}\left(g_i - g_i^{eq}\right) \tag{20}$$

where $f_i = f(t, \vec{x}, \vec{c}_i)$ , $g_i = g(t, \vec{x}, \vec{c}_i)$ and the discrete velocities are given by [10]

$$\vec{c}_i = \begin{cases} (0\,,0) & i = 0 \\ c\left(\cos\left[\frac{\pi(i-1)}{2}\right], \sin[\frac{\pi(i-1)}{2}]\right) & i = 1,2,3,4 \\ \sqrt{2}c\left(\cos\left[\frac{\pi(2i-9)}{4}\right], \sin[\frac{\pi(2i-9)}{4}]\right) & i = 5,6,7,8 \end{cases} \tag{21}$$

with $= \sqrt{3RT}$ . The corresponding discrete equilibrium distribution function, $f_i^{eq}$, can be obtained from Eq. (3) by performing a Taylor expansion up to $\vec{u}^2$ as follows

$$f_i^{eq} = w_i \rho \left[1 + \frac{\vec{c}.\vec{u}}{c_s^2} + \frac{(\vec{c}.\vec{u})^2}{2c_s^4} - \frac{u^2}{2c_s^2}\right] \tag{22}$$

where $c_s = \sqrt{RT}$ is the sound speed and $w_0 = \frac{4}{9}$, $w_i = \frac{1}{9}$ for $i = 1 - 4$ and $w_i = \frac{1}{36}$ for $i = 5 - 8$. Apparently, a comparison between Eq. (17), Eq. (18) and Eq. (22) lead to

$$g^{eq} = T\, f^{eq} \tag{23}$$

and by neglecting the term $O(u^2)$

$$g_i^{eq} = w_i T \left[1 + \frac{\vec{c}.\vec{u}}{c_s^2}\right] \tag{24}$$

The macroscopic variables are now defined by [7]

$$\rho = \sum_{i=0}^{8} f_i \tag{25}$$

$$\rho\vec{u} = \sum_{i=0}^{8} f_i\, \vec{c}_i \tag{26}$$

$$T = \sum_{i=0}^{8} g_i \tag{27}$$

As a result, the discrete velocity Boltzmann BGK Eq. (19) and (20) recover the continuity equation, momentum conservation equation and the following temperature equation [7]

$$\partial T/\partial t + \vec{u}\,.\nabla T = \nabla\,.(\alpha \nabla T) \tag{28}$$

where the thermal diffusivity is $\alpha = \tau_g RT$ .

## 4 SPECIFICATION OF THE PROBLEM

In this study, we solve the velocity and temperature fields using two different distribution functions TLBM for two natural convection heat transfer problems, constant temperature on the walls and adiabatic walls.

The study is carried out numerically for a range of Rayleigh numbers. The governing Eq. (1) to Eq. (8) were discretized and simplified resulting in a system of algebraic equations.

In first case, we evaluate the different models for application of boundary conditions in natural convection phenomena in square cavity.

The thermal conditions applied on the bottom wall is $T_h = 1.0$, top wall is $T_c = 0.0$ and partitioned wall is $T_p = 0.0$. The other faces being adiabatic, $\frac{\partial T}{\partial n} = 0$ , where $\frac{\partial T}{\partial n}$ is the appropriate normal derivative. The temperature difference between the left and right walls introduces a temperature gradient in a fluid, and the consequent density difference induces a fluid motion, that is, convection. In the simulation, the Boussinesq approximation is applied to the buoyancy force term.

$$\rho\vec{G} = \rho\beta g_0(T - T_m)\,\vec{j} \tag{29}$$

where Boussinesq approximation is given by

$$\beta = -\frac{1}{\rho}\left(\frac{\partial\rho}{\partial T}\right)_P \tag{30}$$

and $\beta$ is the thermal expansion coefficient, $g_0$ is the acceleration due to gravity, $T_m$ is the average temperature and $j$ is the vertical direction opposite to that gravity [6].

The dynamical similarity depends on two dimensionless parameters: the Prandtl number, $Pr$ and the Rayleigh number, $Ra$ defined as,

$$\mathrm{Pr} = \frac{\vartheta}{\alpha} \tag{31}$$

$$Ra_L = \frac{\beta g_0(T_H - T_c)L^3}{\vartheta\alpha} \tag{32}$$

The Nusselt number ($Nu$) is one of the most important dimensionless numbers in describing the convective transport. The $Nu$ are averaged and evaluated along the length of cavity which may be expressed as

$$\overline{Nu} = \frac{\bar{h}L}{k_f} = f\,(Re_L\,, Pr) \tag{33}$$

Also about applying of boundary conditions on walls in macroscopic state:

$$\frac{\partial T}{\partial x} = 0 \begin{cases} T(i,j) = T(i+1,j) \\ T(i,j) = \frac{1}{3}[4T(i+1,j) - T(i+2,j)] \end{cases} \tag{34}$$

and when we want to apply them on distribution functions (Appendix I):

$$\frac{\partial T}{\partial x} = 0 \begin{cases} g(i,j,k) = T(i+1,j,k) \quad k = 0,1,2,\dots,9 \\ g(i,j,k) = \frac{1}{3}[4g(i+1,j,k) - g(i+2,j,k)] \quad k = 0,1,2,\dots,9] \end{cases} \tag{35}$$

where in all simulations $\Pr = 0.718$ , grid sizes are 50x50, 100x100, 150x150 for AR=1, 100x50, 200x100, 300x150 for AR=2 and the fluid in a partitioned cavity is air for Ra = $10^3$ - $10^6$.

Wall boundary conditions are used at the all walls of the partitioned cavity, and the non-equilibrium bounce back boundary conditions for velocity. The means of this term is $u = 0.0$ in $x$ direction and $v = 0$ in $y$ direction for all partitioned cavity walls. The bounce-back rule of the non-equilibrium distribution function proposed by Zou and He [14] is used for implementing the boundary condition.

For viscous flows bounce back boundary condition is employed which is equivalent to no slip condition. This boundary condition is employed on wall nodes. Here in the algorithm for performing the bounce-back step for D2Q9 Lattice structure:

$$f_0 = f_0$$
$$f_1 = f_3 , f_2 = f_4$$
$$f_5 = f_7 , f_6 = f_8$$

The thermal conditions applied on the bottom wall is $T_h = 1.0$, top wall is $T_c = 0.0$ and partitioned wall is $T_p = 0.0$. The other faces being adiabatic, $\frac{\partial T}{\partial n} = 0$ , where $\frac{\partial T}{\partial n}$ is the appropriate normal derivative. $H$ is a height of cavity, $W$ is a length of cavity, $h$ is a height of partitioned in the cavity, $C$ is a partition position and $\frac{W}{H}$ means by aspect ratio of the cavity.

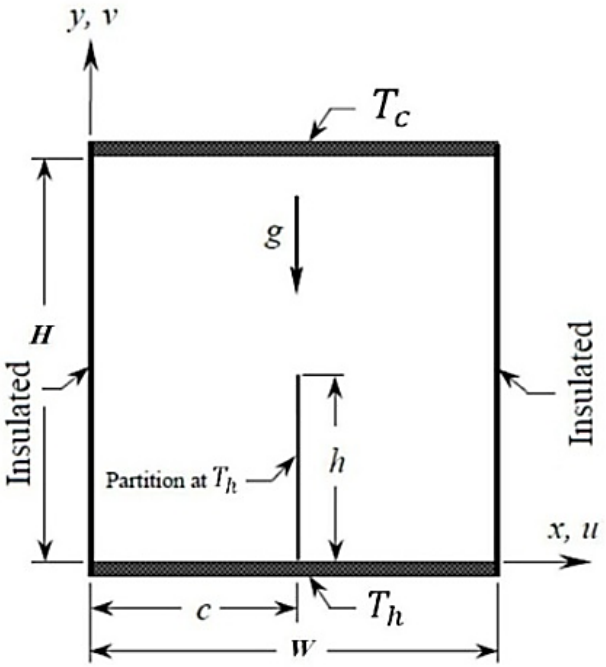


Figure 2: Schematic for the physical model function

## 5 RESULTS AND DISSCUTION

The considered problem is natural convection in a 2D square cavity and enclosure with two horizontal side walls maintained at different temperatures. The temperature difference between the walls introduces a temperature gradient in the fluid, and the consequent density difference induces fluid motion. The remaining walls are adiabatic. The problem definition and the boundary conditions are displayed in Fig. 2.

The non-dimensional heat transfer rate at the isothermal walls is a very important parameter in many engineering applications, such as electronic cooling, transportation, the environment and national security [2]. Numerical simulations of the natural convection in a partition cavity with $AR = 2$ at Rayleigh numbers from $10^3$ to $10^6$ are carried out using the two dimensional particle velocity model of D2Q9.

### 5.1 Isotherms and Streamlines

The streamlines and isothermal contours in the cavity with $AR = 2$ for $C = \frac{W}{5}$ and $\frac{h}{H} = 0.5$ are shown in Figs. 3 and 4 for different Rayleigh numbers from $2 \times 10^4$ to $10^6$ and 100x50 uniform mesh cells. In this figures, the effects of Rayleigh numbers in the flow patterns and isothermals are investigated.

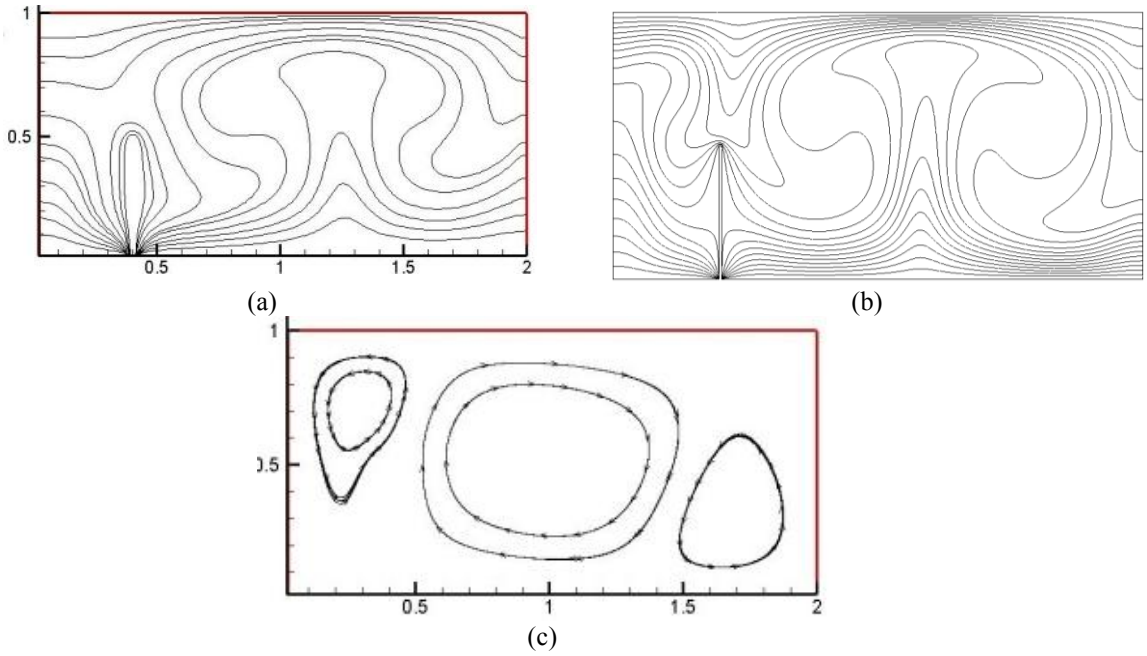


Figure 3: Isotherms with TLBM (a), Isotherms with CFX (b) and Streamlines with TLBM (c) for $Ra = 2 \times 10^4$, $AR = 2$, $C = \frac{W}{5}$, $\frac{h}{H} = 0.5$ and 100x50 uniform mesh cells

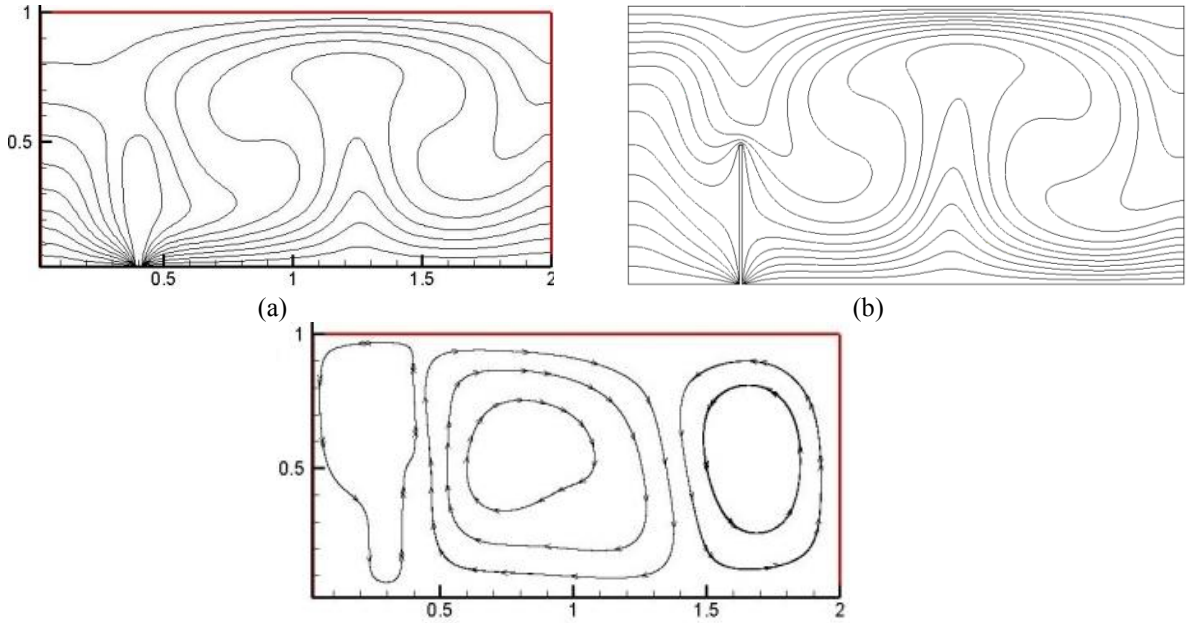


Figure 4: Isotherms with TLBM (a), Isotherms with CFX (b) and Streamlines with TLBM (c) for $Ra = 10^6$, $AR = 2, C = \frac{W}{5}, \frac{h}{H} = 0.5$ and 100x50 uniform mesh cells

Table 1 shows the macroscopic values on the partitioned cavity at $Ra = 2 \times 10^4$, $AR = 2, C = \frac{W}{5}$, $\frac{h}{H} = 0.5$ and 100x50 uniform mesh cells using D2Q9 lattice structure when we apply boundary conditions on thermal distribution function (method No.1) and macroscopic temperature directly (method No.2).

Table 1: Properties of some nodes for $Ra = 2 \times 10^4$, $AR = 2, C = \frac{W}{5}$, $\frac{h}{H} = 0.5$ and 100x50 uniform mesh

| $x$ | $y$ | $u$ | $v$ | $\rho$ | T (method 1) | T (method 2) |
|---|---|---|---|---|---|---|
| 0.056 | 0.0522 | 0.0012 | 0.0007 | 1.0361 | 0.8104 | 0.8406 |
| 0.344 | 0.0488 | 0.0013 | 0.0004 | 1.0352 | 0.6084 | 0.6084 |
| 0.081 | 0.9350 | 0.0009 | 0.0006 | 0.9833 | 0.0045 | 0.0045 |
| 0.441 | 0.3190 | 0.0005 | 0.0008 | 1.0034 | 0.0331 | 0.0331 |
| 0.715 | 0.6030 | 0.0121 | 0.0270 | 0.9915 | 0.3864 | 0.3864 |
| 1.206 | 0.3770 | 0.0011 | 0.0001 | 1.0017 | 0.0936 | 0.0936 |
| 1.777 | 0.4820 | 0.0088 | 0.0513 | 0.9963 | 0.3138 | 0.3138 |

The streamlines in Figs. 3 and 4 show as $Ra$ increases, the flow rate toward partitioned enclosure increases. The agreement of numerical results of isotherms and streamlines between TLBM and international previous literature is very good [2, 10].

For small $Ra$ cases, the fluid motion driven by the buoyancy force is very slow, leading to rather weak natural convection in the enclosure. On the other hand, when $Ra$ number increase, the buoyancy force accelerates the fluid flow and natural convection is significantly enhanced. This behavior is clearly similar to the related flow pattern in all ranges of $Ra$ and buoyancy parameter. The above discussed behaviors are also found in the previous experimental and numerical studies [2, 6].

### 5.2 Grid-Independency of the Results

In order to see the influence of the grid size on the $\overline{Nu}$ at the isothermal walls, the numerical simulations for $Ra = 2 \times 10^4$ using D2Q9 are carried out on three different grid sizes for all models in the following section, 50x50, 100x100 and 150x150 for portioned cavity with $AR = 1$ , $c = \frac{W}{2}$ , $\frac{h}{H} = 0.5$ and 100x50, 200x100 and 300x150 for portioned cavity with $AR = 2$ , $c = \frac{W}{2}$ , $\frac{h}{H} = 0.5$. Tables 2 and 3 show the values of Average Nusselt number ($\overline{Nu}$) are independent from the number of mesh cells.

Table 2: Ave. Nusselt number values for partitioned cavity with $Ra = 2 \times 10^4$ , $AR = 2$ , $C = \frac{W}{5}$, $\frac{h}{H} = 0.5$.

| Grid | 50x50 | 100x100 | 150x150 |
|---|---|---|---|
| $\overline{Nu}$ | 1.091 | 1.085 | 1.087 |

Table 3: Ave. Nusselt number values for partitioned cavity with $Ra = 2 \times 10^4$ , $AR = 2$ , $C = \frac{W}{5}$, $\frac{h}{H} = 0.5$.

| Grid | 100x50 | 200x100 | 300x150 |
|---|---|---|---|
| $\overline{Nu}$ | 1.005 | 1.006 | 1.005 |

### 5.3 Comparison of Average Nusselt Number

The $Nu$ obtained in this work, the previous experimental data [11] and the previous numerical results are compared [2, 12, 13] are compared in Table 4. It is seen that the numerical results obtained by the present TLBM agree well with those reported in the previous studies for different $Ra$ numbers mentioned here.

Table 4: Comparison of the average Nusselt number at the isothermal walls between TLBM and previous works partitioned cavity with $AR = 1$ , $C = \frac{W}{2}$ , $\frac{h}{H} = 0.5$ and 50x50 uniform mesh cells

| | Present study | Anilkumar [2] | Barakos [11] | Devahl Davis [12] | Fusegi [13] |
|---|---|---|---|---|---|
| $(Ra = 10^3)$ $\overline{Nu}$ | 1.091 | 1.152 | 1.114 | 1.118 | 1.105 |
| $(Ra = 10^5)$ $\overline{Nu}$ | 4.204 | 4.636 | 4.51 | 4.519 | 4.646 |
| $(Ra = 10^6)$ $\overline{Nu}$ | 8.526 | 9.241 | 8.806 | 8.799 | 9.012 |

Table 5: Average Nusselt number at the isothermal walls for partitioned cavity with $AR = 2$ , $C = \frac{W}{2}$ , $\frac{h}{H} =$ 0.5 and 100x50 uniform mesh cells

| | Present study |
|---|---|
| $(Ra = 10^3)$ $\overline{Nu}$ | 1.0004 |
| $(Ra = 10^5)$ $\overline{Nu}$ | 2.0040 |
| $(Ra = 10^6)$ $\overline{Nu}$ | 2.8240 |

From the results presented above, we can say that as the $Ra$ number increase, the $\overline{Nu}$ at the isothermal walls of partitioned cavity increase. It is shown that the $\overline{Nu}$ at the isothermal walls is increased as the aspect ratio decreased. The numerical results agree well with other results reported in the previous studies [2].

## 6 CONCLUSIONS

A two dimensional incompressible TLBM using D2Q9 lattice structure was proposed in this work. The study was carried out numerically for a range of Rayleigh numbers, partition heights and aspect ratio of the cavity. The numerical results of this model for simulation of 2D natural convection heat transfer of air in a partitioned cavity with different aspect ratio compared well with those from previous works. We have shown that based on computer codes and mixed program (i.e. TLBM with another methods), we can use both of types of applying the boundary conditions with minimum term of derivatives that reported in similar works. Also the results showed that as the $Ra$ number increase, $\overline{Nu}$ at the isothermal walls of cavity increased and $\overline{Nu}$ at the isothermal walls is increased as the aspect ratio decreased.

## APPENDIX I

$$\frac{\partial T}{\partial x}=0 \begin{cases} g(i,j,0)=g(i+1,j,0) \quad or \quad g(i,j,0)=\frac{1}{3}[4g(i+1,j,0)-g(i+2,j,0)] \\ g(i,j,1)=g(i+1,j,1) \quad or \quad g(i,j,1)=\frac{1}{3}[4g(i+1,j,1)-g(i+2,j,1)] \\ g(i,j,2)=g(i+1,j,2) \quad or \quad g(i,j,2)=\frac{1}{3}[4g(i+1,j,2)-g(i+2,j,2)] \\ g(i,j,3)=g(i+1,j,3) \quad or \quad g(i,j,3)=\frac{1}{3}[4g(i+1,j,3)-g(i+2,j,3)] \\ g(i,j,4)=g(i+1,j,4) \quad or \quad g(i,j,4)=\frac{1}{3}[4g(i+1,j,4)-g(i+2,j,4)] \\ g(i,j,5)=g(i+1,j,5) \quad or \quad g(i,j,5)=\frac{1}{3}[4g(i+1,j,5)-g(i+2,j,5)] \\ g(i,j,6)=g(i+1,j,6) \quad or \quad g(i,j,6)=\frac{1}{3}[4g(i+1,j,6)-g(i+2,j,6)] \\ g(i,j,7)=g(i+1,j,7) \quad or \quad g(i,j,7)=\frac{1}{3}[4g(i+1,j,7)-g(i+2,j,7)] \\ g(i,j,8)=g(i+1,j,8) \quad or \quad g(i,j,8)=\frac{1}{3}[4g(i+1,j,8)-g(i+2,j,8)] \end{cases}$$

## REFERENCES

[1] C. S. Nor Azwadi and A.R.M. Rosdzimin, Simulation of natural convection heat transfer in an enclosure using lattice Boltzmann method, Jurnal Mekanikal, 2008, No. 27, 42 - 50.

[2] S. H. Anilkumar and G. Jilani, Natural convection heat transfer enhancement in a closed cavity with partition utilizing Nano fluids, Proceedings of the World Congress on Engineering 2008 Vol II, WCE 2008, July 2 - 4, 2008, London, U.K.

[3] Y. Peng, C. Shu and Y.T. Chew, A 3D incompressible thermal lattice Boltzmann model and its application to simulate natural convection in a Cubic Cavity, Journal of Computational Physics 193 (2003) 260–274.

[4] Z. Guo and T.S. Zhao, Lattice Boltzmann simulation of natural convection with temperature-dependent viscosity in a porous cavity, Progress in Computational Fluid Dynamics, Vol. 5, Nos. 1/2, 2005.

[5] T. changing, H Yaling, W. Yong and L. Yingwen, Simulation of transient natural convection in square cavity with incompressible thermal lattice-Boltzmann method, JOURNAL OF XI'AN JIAATONG UNIVERSITY, vol.41 No.1, Jan 2007.

[6] C. S. Nor Azwadi and T. Tanahashi, Development of 2-D and 3-D double-population thermal lattice Boltzmann models, MATEMATIKA, 2008, Volume 24, Number 1, 53-66.

[7] Y. Shi, T.S. Zhao and Z.L. Guo, Finite difference-based lattice Boltzmann simulation of natural convection heat transfer in a horizontal concentric annulus, Computers & Fluids 35 (2006) 1–15.

[8] S. Harris, Holt, Rinehart and Winston, An introduction to the theory of the Boltzmann equation, Holt, Rinehart and Winston, New York, 1971.

[9] C. Cercignani, The Boltzmann equations and its application, in Applied Mathematical Sciences, Springer-Verlag, New York, 1988.

[10] Y. H. Zhang, X. Jun, R. W. Barber and D. R. Emerson, A thermal lattice Boltzmann Model for Low speed rarefied gas flow, Council for the Central Laboratory of the Research Councils, DL-TR-2006-002.

[11] G. Barakos and E. Mitsoulis, Natural convection flow in a square cavity revisited: laminar and turbulent models with wall functions, Int. J. Numer. Methods Fluids, vol.18, 1994, pp.695-719.

[12]. G. De. Vahl Davis, Natural convection of air in a square cavity: a bench mark numerical solution, Int. J. Numer. Methods Fluids, vol.3, 1983, pp.249-264.

[13] T. Fusegi, J.M. Hyuna, K. Kuwahara and B. Farouk, A numerical study of 3D natural convection in a differentially heated cubical enclosure, Int.J.HMT, vol.34, 1991, pp.1543-1557.